The Role of Backscattering in SHG Tissue Imaging

François Légaré,* Christian Pfeffer,[†] and Bjorn R. Olsen[†]
*Center for Nanoscale Systems, Harvard University, Cambridge, Massachusetts; and [†]Harvard School of Dental Medicine, Boston, Massachusetts

ABSTRACT   We investigate the properties of second-harmonic generation (SHG) tissue imaging for the functional biological unit fascia, skeletal muscle, and tendon. Fascia and Achilles tendon primarily consist of similar collagen type I arrays that can be imaged using SHG microscopy. For muscle, it is the myosin molecules represented within the A bands. For fascia and tendon tissue samples, we observe, in addition to a stronger signal in forward images, vastly different features for the backward versus the forward images. In vivo as well as intact ex vivo thick tissue imaging requires backward detection. The obtained image is a result of the direct backward components plus a certain fraction of the forward components that are redirected (backscattered) toward the objective as they propagate within the tissue block. As the forward and the backward images are significantly different from each other for the imaged collagen type I tissue, it is crucial to determine the fraction of the forward signal that contributes to the overall backward signal. For intact ex vivo SHG imaging of Achilles tendon, we observe a significant contribution of forward features in the resulting image. For fascia, the connective tissue immediately surrounding muscle, we only observe backward features, due to low backscattering in muscle.

INTRODUCTION

Multiphoton microscopy, a form of laser scanning microscopy (1), has established itself as a powerful technique for in vivo imaging (2–6). In its most commonly used form, an intense near-infrared ultra-short laser pulse interacts nonlinearly with the sample, giving efficient excitation of the fluorophores only at the focus of the objective, providing submicron resolution. The use of near-infrared sources allows deep tissue (7–9) and live animal imaging (10,11) (see (12) for an extensive review of multiphoton microscopy and its applications). This has proven invaluable for studying cell-cell interaction, physiology, and morphology in tissues (13–16).

Despite its many advantages for in vivo tissue imaging, the reliance on intrinsic and extrinsic fluorophores leads inevitably to the effects of phototoxicity and photobleaching, limiting the application. To circumvent those limitations, other nonlinear optical techniques have been demonstrated for tissue imaging, such as second-harmonic generation (17–23), third-harmonic generation (24–26), and coherent anti-Stokes Raman scattering (27,28). These techniques do not involve electronic population transfer, avoiding problems associated with fluorescence microscopy.

In general, noncentrosymmetric structures are required for second harmonic generation. In 1978, Freund et al. (29) have shown that the interaction of an intense laser pulse with noncentrosymmetric structures such as collagen matrices produces second-harmonic generation (SHG). The application of SHG in microscopy has been used to successfully image structural protein arrays from various nonanimal and animal sources such as insects, nonvertebrates, and vertebrates (19, 30–32). With collagen types I and III as the forerunners, actomyosin and tubulin scaffolds have been imaged.

Collagen type I is the most abundant structural protein in higher vertebrates. Structural changes in its composition and fibrillar matrix are associated with physiological and disease processes during development, growth, remodeling, repair, aging, diabetes, cancer, and wound healing (33–37).

In this article, we investigate SHG imaging of the biological functional unit of skeletal muscle, its fascia and Achilles tendon in mouse. We investigate specifically fascia and Achilles tendon, as both have histologically a very similar collagen type I architecture, although the concentration and diameter size vary. We observe that these histologically similar tissues result in vastly different SHG images. We show that these whole and intact thick tissue SHG images depend strongly on the optical properties of the tissue.

EXPERIMENTAL METHODS

Sample preparation

Five male C57/B6 mice, six weeks of age were sacrificed; whole hind legs were harvested and fixed in 4% PFA for 6–8 h at 4°C. Fascia was separated from skeletal muscle under a Nikon dissecting scope with 0.7–8× zoom lens. The thin fascia (~10 μm thick) tissue was immediately transferred onto 100-μm thick coverslips (VWR International, West Chester, PA; 24 mm × 60-mm, No. 1) treated with 3-aminopropyltriethoxysilane or gelatin-chromium potassium sulfate solution (gelatin type A, and chromium potassium sulfate; both Sigma, St. Louis, MO) for optimal tissue adhesion. For the whole, thick tissue sample, the skin was removed from the hind legs. The fascia and gastrognemicus muscle tissue block was exposed and imaged directly with SHG.

Achilles tendon (*Tendo calcaneo*) was harvested from the aforementioned mice under a Nikon dissection scope (Melville, NY). The tissue blocks were embedded in OCT-compound Tissue-Tek (Electron Microscopy Sciences,

Hatfield, PA) and prepared for frozen sectioning. The embedded tissue was sectioned at 10 μm using a Leica cryostat CM3000 (Leica Microsystems, Wetzlar, Germany). The sections were transferred to the coated coverslips mentioned above.

Achilles tendon was exposed in its full length after removal of the skin from the hind legs under the dissecting scope. Due to the protruding calcaneus of the mouse foot, which prevents a flat and immediate surface contact of the intact thick tendon with the coverslip, we excised the tendon-tissue block, ~2-mm thick, and 5-mm long in toto.

For 10-μm skeletal muscle tissue sections, we excised a 5×5 mm tissue block from the gastrognemicus muscle of mouse hind leg, embedded in OCT and sectioned using the Leica cryostat. For thick skeletal muscle tissue, we imaged the gastrognemicus muscle directly, without fascia.

Imaging system

The laser system used to generate second harmonic is a mode-locked Ti:Sapphire laser (~140 fs pulse, 76 MHz repetition rate; MIRA 900-F; Coherent Radiation, Santa Clara, CA) pumped with 5 W from a Verdi laser (Coherent Radiation). The duration of the laser pulse has been measured before it enters the microscope with an autocorellator (APE, Berlin, Germany). For all experiments, the laser wavelength is set at 830 nm (measured with Wave Scan from APE). The beam exiting the laser is deflected into the NIR port of an inverted Axiovert 200 M microscope (Carl Zeiss MicroImaging, Thornwood, NY) and scanned across the sample with the LSM 510 scanning module (Carl Zeiss). The beam is focused into the sample with a $20\times$ dry objective, Plan-Apochromat, $NA = 0.75$ (Carl Zeiss).

For thin sample imaging, we image the samples in two directions, i.e., forward and backward. In both directions, the signal is filtered with a band-pass filter 415 ± 15 nm (Chroma Technology, Rockingham, VT) and a 2-mm-thick BG39 filter. In the backward direction, the signal is deflected toward the external PMT (photomultiplier tube, NDD detector, Carl Zeiss) using a dichroic mirror (long-pass 700 nm, Chroma Technology) placed in the reflector turret of the Axiovert 200 M. The images we present in this article have 1024×1024 pixels, the scanning time per pixel is 0.64 μs and each line is scanned 16 times on average. The detector gain is set constant for all our measurements. In the forward direction, the signal is collected with a $40\times$ water immersion objective, C-Achroplan NIR, $NA = 0.8$ (Carl Zeiss). The optical characteristics of our objective-condenser combination is functionally identical to the one used by Williams et al. to measure F/B ratio of rat tail tendon (21). For the background, an image is taken with no sample in focus and without changing the laser parameters.

In the next section, we present various signal ratios. For thin samples, we measure the average pixel signal in forward (F) and backward (B) detection scheme. The background average pixel signal is subtracted from the average pixel signal of the obtained image. These results are analyzed with ImageJ software (38). The efficiency ratio between forward and backward detection has been calibrated using two-photon fluorescence from coumarin-440 using the same filter combination as the one use for SHG imaging. This F/B ratio is 0.59. All our F/B measurements are calibrated with this value.

To quantify backscattering from thick tissue, the backward signal from thick samples (T) is compared to the backward signal from thin samples (T/B). For thick sample imaging, we assure immediate contact with the cover-slip to prevent laser power loss until light reaches the tissue structures of interest. This measurement, together with the F/B ratio, allows us to determine the fraction of forward signal contributing to the overall backward signal due to backscattering.

To mimic backscattering, the signal is measured in backward signal after adding a thick layer (~10 mm) of 20% intralipid emulsion (Sigma, Cat. No. I-141, Sigma Aldrich, St. Louis, MO) on top of our thin samples (LE). The imaging system is an inverted microscope; therefore, the laser beam does not propagate into the emulsion before interacting with the sample. The emulsion is added to provide scattering of the forward SHG components. This signal is compared to the backward signal from a thin section (LE/B).

The signal (S) strength changes with regard to detection configuration (forward versus backward) as well as sample type (fascia, skeletal muscle,

Achilles tendon). The detector gain is set constant for all our measurements. The laser power has to be adjusted for each measurement to avoid saturation of the PMT signal. The SHG signal is proportional to the square of the intensity. Therefore, we normalize the signal to the square of the laser power (P). The different ratios presented are given by

$$\frac{F}{B} = \frac{S_F}{0.59\,S_B}\left(\frac{P_B}{P_F}\right)^2, \tag{1}$$

$$\frac{LE}{B} = \frac{S_{LE}}{S_B}\left(\frac{P_B}{P_{LE}}\right)^2. \tag{2}$$

$$\frac{T}{B} = \frac{S_T}{S_B}\left(\frac{P_B}{P_T}\right)^2. \tag{3}$$

The imaging of tissues is performed with $1\times$ buffered salt solution (PBS) added to the sample to prevent drying artifacts. In our case, with the solution added to the sample, the solution-air interface results in a large refractive index difference causing Fresnel reflection. This particular reflection affects the F/B ratios the most. To properly assess these ratios, the contribution of this Fresnel reflection to the backward signal has to be suppressed. This is achieved by adding a thick column (5 cm) of PBS on top of the sample moving the PBS-air interface away from the objective suppressing the collection of this Fresnel reflection contribution. In Fig. 1, we present forward and backward images of Achilles tendon demonstrating the effect of Fresnel reflection and its suppression. The image features and the different ratios will be explained in Results. With a thin film of PBS on top of the sample, Fig. 1 *a* has been detected in forward and Fig. 1 *b* in backward mode. Due to Fresnel reflection, forward features from Fig. 1 *a* are evident in Fig. 1 *b*. For Fig. 1 *c*, a thick column (5 cm) of PBS was added on top of the sample, eliminating the contribution of reflected forward components at the PBS-air interface.

RESULTS

In our study, we image the closely cooperating, functional biological unit of Achilles tendon, skeletal muscle, and fascia using second-harmonic generation. We focus on fascia, a sheet-like tissue sheath surrounding muscle groups, and Achilles tendon. Both provide a similar collagen type I architecture, but are embedded in different tissue environments.

Tendo calcaneo SHG imaging

In Fig. 2, we present SHG images from a thin section of Achilles tendon (thickness ~10 μm) and an excised thick, whole tendon block. First, we describe the results obtained from the thin section. Fig. 2 *a* shows the SHG image captured with forward detection. We observe a continuous sheet of parallel collagen fibrils. In Fig. 2 *b*, the same section is imaged in the backward direction. Here, sheet-like collagen structures are observed; however, the continuous fibrillar collagen structures observed in the forward direction are absent whereas heterogeneous submicron features predominate.

This strong difference between forward and backward features is due to the coherent nature of the SHG process. For SHG, the electromagnetic components generated in the focal volume add coherently. Our findings demonstrate that the submicron architecture of collagen is complex. In the backward direction, the coherent addition is strongly affected by
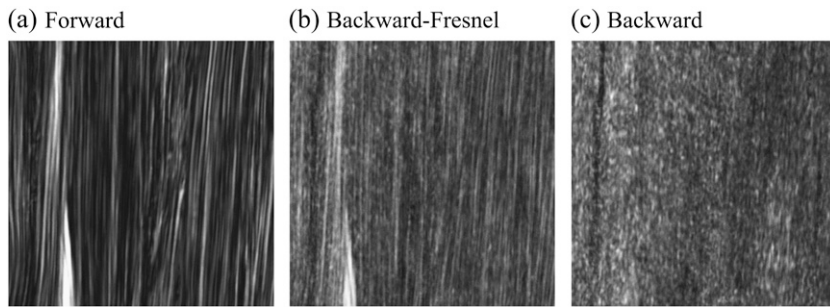
FIGURE 1 SHG images of thin section (~10 μm) of Achilles tendon. (*a*) Forward image. (*b*) Backward image with thin film of PBS (Fresnel reflection is important at the PBS-air interface). (*c*) Backward image with a thick column (5 cm) of PBS on top of the sample (the contribution of Fresnel reflection is suppressed).

the submicron architecture of the collagen matrix. To illustrate this, we discuss a simplified example of two infinitely small scatterers located in the focal volume and distributed along the axis of laser propagation. Modulation of the axial distance between the two scatterers on the spatial scale of $\lambda_{SHG}/2$ (210 nm) will strongly modulate the signal in the backward direction (21). Collagen arrays are much more complex than are two small scatterers. However, similar to our simplified example, the axial distribution of collagen is modulated, as the architecture at the submicron level is not uniform and continuous (21). Collagen type I structures such as Achilles tendon are made primarily of collagen I molecules, ~300-nm long and 1.5 nm in diameter. These molecules form polymers of various densities and diameters that make the overall collagen scaffold architecture (39–41), leading to the observation of heterogeneous submicron features in backward.

It has been demonstrated that tissues can provide significant backscattering of the forward components (26,28). We mimic this mechanism by adding a 20% intralipid emulsion, a highly scattering medium, on top of the thin tendon section. The backward image in Fig. 2 *c*, after adding intralipid

emulsion, shows continuous collagen structures (Fig. 2 *a*) as well as heterogeneous submicron features (Fig. 2 *b*). It represents a combination of both images, Fig. 2, *a* and *b*. The forward SHG features observed in Fig. 2 *c* suggests that a significant fraction of forward components are backscattered and efficiently collected in backward components. For whole, thick tendon tissues (Fig. 2 *d*), the image strongly resembles Fig. 2 *c*, suggesting that thick tendon, similar to the emulsion, provides a highly scattering medium.

To quantify our observations, we image thin tendon sections as well as thick, whole ex vivo tendon tissue from five different age-matched male C57/B6 mice. From the obtained signals, we determine the various ratios outlined in Experimental Methods. These ratios allow us to assess the fraction of forward signal contributing to the overall backward signal due to backscattering.

For thick tissue imaging, as well as our scattering model (20% intralipid emulsion), the measured signal is a result of the direct backward components plus a certain fraction of forward components redirected toward the objective and detected. Therefore, the ratio T/B is
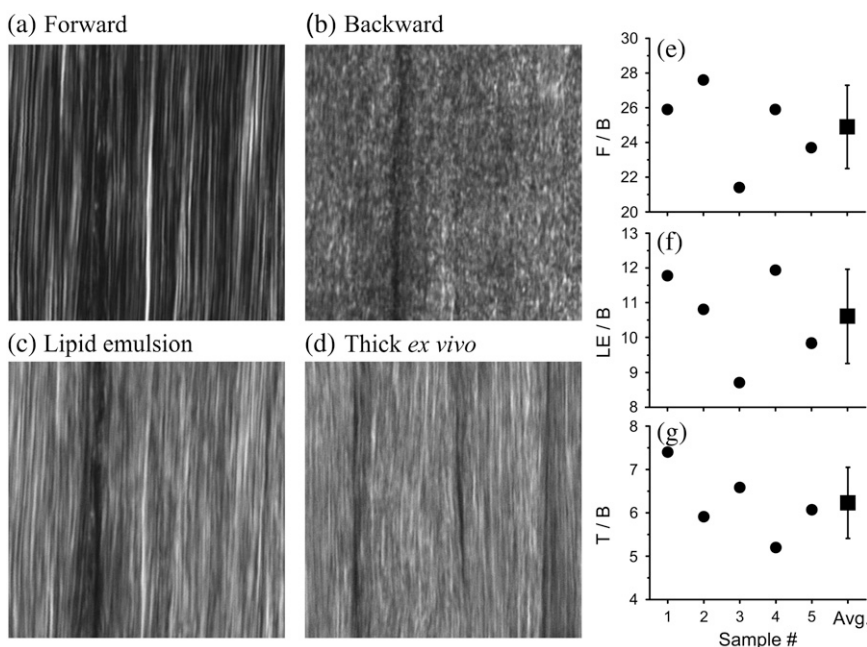

FIGURE 2 SHG images and ratio measurements for Achilles tendon. (*a–c*) Approximately 10 μm sample thickness. (*a*) Forward image. (*b*) Backward image. (*c*) 20% Intralipid emulsion added onto the thin sample section. (*d*) Image of thick intact, ex vivo tissue block (~5 mm thickness). All images have 1024 × 1024 pixels and the dimension is $x = 67$ μm and $y = 67$ μm. The image of the intact, thick tendon tissue (*d*) strongly resembles the image obtained with intralipid emulsion on top of a thin sample section (*c*), suggesting that backscattering is important for Achilles tendon imaging. Ratio measurements are (*e*) *F/B*, (*f*) *LE/B*, and (*g*) *T/B*. These ratios are outlined in Experimental Methods. The average ratios are *F/B* = 24.9 ± 2.4, *LE/B* = 10.6 ± 1.4, and *T/B* = 6.2 ± 0.8. These ratios are used to determine the fraction of forward signal contributing to the overall backward signal due to backscattering. For whole, thick ex vivo tendon, $P_{bs} = 21 ± 6\%$. Adding a 20% intralipid emulsion on top of the thin sample section, $P_{bs} = 39 ± 10\%$.

$$\frac{T}{B} = \frac{P_{bs}S_F^T + S_B^T}{S_B},$$ (4)

where P_{bs} is the fraction of forward signal contributing to the overall backward signal due to backscattering, and S_F^T and S_B^T are the forward and the backward signals from the thick tissue block. The value S_B is the backward signal from the thin sample. To determine P_{bs}, we assume that on average, the forward signal generated in thin tissue sections equals the signal generated in thick tissue. The same assumption applies for the backward signal, therefore

$$P_{bs} = \frac{(T/B - 1)}{F/B}.$$ (5)

For the experiments that imitate backscattering, P_{bs} is assessed by replacing T/B ratio with LE/B.

In Fig. 2, e–g, we present the ratios needed to obtain P_{bs}. Fig. 2 e presents the F/B ratio for our five measurements. The average value obtained for the F/B ratio is 24.9, confirming that the forward signal is stronger than the backward signal (20,21). For the LE/B ratio, we get an average value of 10.6 confirming that the 20% intralipid emulsion provides significant backscattering of the forward components (Fig. 2 f). Using the F/B and the LE/B ratios, we determine that the fraction of forward signal contributing to the overall backward signal due to backscattering is $P_{bs} = 39\%$.

For intact, whole thick tendon, we observe that $T/B = 6.2$ (Fig. 2 g). Using Eq. 5, we determine that 21% of the forward signal contributes to the overall backward signal. To understand the SHG image formation of collagen type I tissue scaffolds, we investigate structures that are similar to Achilles tendon in architecture but embedded in different tissue environments.

Fascia imaging

In Fig. 3, we present SHG images from explanted gastrognemicus fascia tissue (thickness $\sim$10 μm) and excised fascia-muscle tissue block. The SHG image captured in the forward direction shows continuous sheets of parallel collagen fibrils highly resembling SHG images of thin tendon sections (Fig. 3 a). These features are absent in the backward direction (see Fig. 3 b); instead, heterogeneous submicron collagen features are observed. We mimic backscattering for the thin fascia section by adding a 20% intralipid emulsion. Comparable to tendon, the resulting image is a combination of the image captured in the forward (Fig. 3 a) and the backward direction (Fig. 3 b).

Fig. 3 d represents an SHG image from an intact ex vivo fascia-muscle tissue block, taken $\sim$3 μm into the fascia to obtain maximum signal strength. The observed features show primarily heterogeneous submicron features, highly similar to those in Fig. 3 b, indicating that forward components are not contributing significantly to the image formation.

To support our qualitative results, we determine the F/B and T/B ratios as presented in Fig. 3, e–g. For the F/B, our

five measurements average 4.2 (Fig. 3 e), and the LE/B ratio equals 2.7 (see Fig. 3 f). Since the F/B ratio for fascia is small, the contribution of Fresnel reflection at the PBS-air interface to the backward signal is extremely weak. For thin fascia section plus 20% intralipid emulsion on top, using Eq. 5, we determine that the fraction of forward signal contributing to the overall backward signal due to backscattering is $P_{bs} = 41\%$.

For our intact, ex vivo fascia-muscle tissue blocks, we determine that $T/B = 1.1$ (Fig. 3 g). This result indicates that the signal from thin and thick, intact fascia tissue block are nearly equal. From the ratios presented in Fig. 3, e and g, we determine that the fraction of forward signal contributing to the overall backward signal due to backscattering is $P_{bs} = 2\%$. This strongly suggests that the tissue surrounding fascia does not provide significant backscattering of the forward components.

Fascia in mouse muscle tissue is $\sim$10-μm thick and cannot by itself provide significant backscattering. Based on histological and anatomical data, the only tissue remaining that could provide any significant backscattering would be skeletal muscle. Previous studies have demonstrated that muscle can be imaged using SHG microscopy (17,23,24). The SHG signal is generated by the interaction of the laser pulse with thick myosin II filaments within the A bands (23). To confirm the histological description mentioned above, that fascia and muscle tissue are in close proximity, we present in Fig. 4 an SHG image of the fascia muscle interface. The first muscle interface appears $\sim$10 μm after the last fascia focal plane. The space between fascia and muscle is filled with mostly loose connective tissue and microvasculature. To investigate whether muscle can provide any significant backscattering of the SHG fascia forward components, we assess F/B and T/B from thin and thick skeletal muscle samples, respectively (see Fig. 5).

The F/B ratio for our thin muscle sections ($\sim$10 μm) is 478 (Fig. 5 a). Due to the very large F/B ratio, it is critical to suppress from the backward signal the contribution of Fresnel reflection at the PBS-air interface. For T/B, we then obtain 4.9 (Fig. 5 b). For whole excised thick muscle tissue block, the fraction of forward signal contributing to the overall backward signal is $P_{bs} = 0.8\%$.

Fig. 5 c is a backward image of a thin muscle section. Fig. 5 d is an image of thick whole ex vivo muscle. Backscattering in skeletal muscle is weak, and since the F/B ratio for fascia is small (4.2), forward features are absent for fascia images (see Fig. 3 d).

Without suppressing the contribution of the Fresnel reflection to the backward signal for thin muscle section, we observe that the T/B ratio is the range of 1. In this case, the amount of forward signal reflected at the PBS-air interface is $P_{bs} = 0.8\%$. This wrongly leads to the interpretation of absent backscattering in skeletal muscle and that the SHG image formation is only due to the direct backward signal.
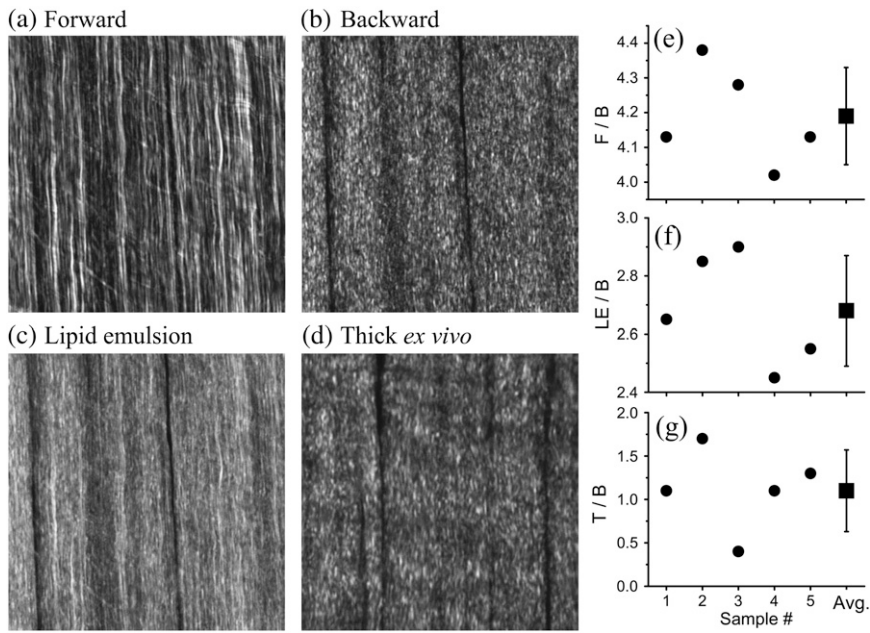
(a) Forward (b) Backward

(c) Lipid emulsion (d) Thick *ex vivo*

FIGURE 3 HG images and ratio measurements for fascia. (*a–c*) Approximately 10 μm sample thickness. (*a*) Forward image. (*b*) Backward image. (*c*) 20% Intralipid emulsion added on sample section. (*d*) Fascia-muscle intact, thick ex vivo tissue block (~5 mm thickness). All images have 1024 × 1024 pixels and the dimension is $x = 92$ μm and $y = 92$ μm. The image of the thick ex vivo tissue (*d*) strongly resembles the backward image (*b*). Both exhibit almost exclusively submicron features in contrast to the model backscattered fascia image (*c*). Ratio measurements are (*e*) F/B, (*f*) LE/B, and (*g*) T/B. The ratios are outlined in Experimental Methods. The average ratios are $F/B = 4.2 \pm 0.1$, $LE/B = 2.7 \pm 0.2$, and $T/B = 1.1 \pm 0.4$. These ratios are used to determine the fraction of forward signal contributing to the overall backward signal due to backscattering. For thick ex vivo fascia, $P_{bs} = 2 \pm 11\%$. Adding a 20% intralipid emulsion on top of the thin sample section, $P_{bs} = 41 \pm 7\%$.

In SHG, the incident light interacts nonlinearly with the sample at the focal volume. However, the generated light after the focus is impacted by the linear optical properties of the immediate surrounding environment. To explain the effect of strong backscattering of the SHG forward components in thick tendon tissue and its weakness in skeletal muscle, we consult studies that investigate light propagation in similar tissues as well as intralipid emulsion. To assess the light propagation in tissues, the reduced scattering coefficient (μ_s') is determined as a means to indicate how effectively the corresponding tissues scatter light (41).

Chen et al. (42), as well as van Staveren et al. (43), determined the reduced scattering coefficient within the spectral ranges of visible to infrared light for intralipid emulsion, very similar to the emulsion used for our experiments. Based on their results, we infer that, at 410 nm, the reduced scattering coefficient for 20% intralipid emulsion will be $\mu_s' \sim 300$ cm^{-1}. These results clearly demonstrate that this emulsion scatters light strongly and provides efficient and very strong backscattering of forward components. Other studies confirm this (28).
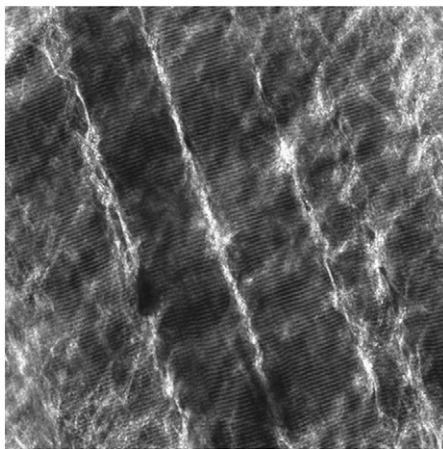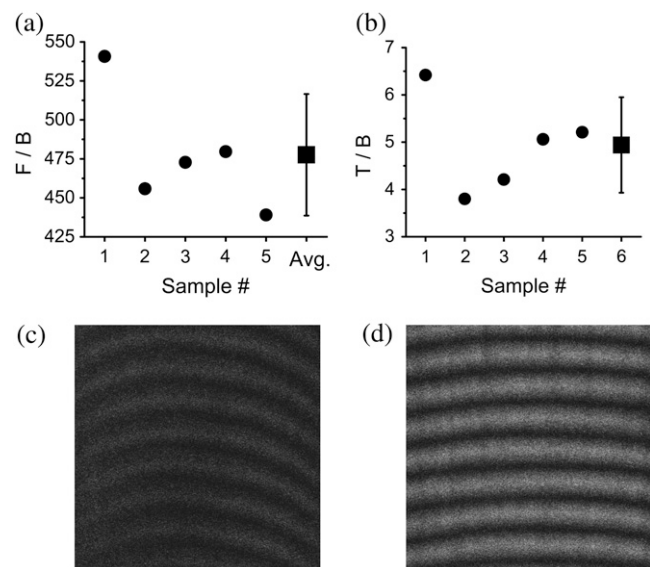

FIGURE 5 Ratio measurements for determining the amount of backscattering for muscle, (*a*) F/B and (*b*) T/B. These ratios are outlined in Experimental Methods. The average ratios are $F/B = 478 \pm 39$ and $T/B = 4.9 \pm 1$. With these ratios, we determine that the probability of backscattering for muscle is $P_{bs} = 0.8 \pm 0.3\%$. (*c*) Backward image of a thin section (~10 μm) of skeletal muscle ($x = 18$ μm and $y = 18$ μm). (*d*) Thick ex vivo image of an intact muscle tissue block (same dimension as in *c*).

FIGURE 4 SHG image from fascia-muscle tissue block interface. It has been taken ~10 μm into the tissue from the last fascia focal plane. The image have 1024 × 1024 pixels and the dimension is $x = 230$ μm and $y = 230$ μm.

As for the reduced scattering coefficient of skeletal muscle, Marquez et al. (44) investigated light propagation in skeletal muscle of chicken breast tissue. Their findings show that the reduced scattering coefficient depends slightly on the orientation of the muscle striation to the incident laser propagation axis. At 410 nm, they measure $\mu_s' \sim 3 \text{ cm}^{-1}$— indicating that skeletal muscle scatters light weakly, leading to weak backscattering. Albeit these measurements have been done in chicken breast tissue, we can assume very similar results for mouse skeletal muscle because the histological and ultrastructural, as well as biochemical composition, are nearly identical.

To determine the scattering properties of Achilles tendon, we refer to Saidi et al. (41), who investigated light scattering in human neonatal skin at different gestational periods. The dermis of mature skin is composed of a dense meshwork of collagen type I fibrils lending the skin its mechanical strength. The density of this collagen architecture is comparable to Achilles tendon, although the collagen fibril alignment in tendon is different from dermis as it is only along the main force axis. At full maturity, 52 weeks, Saidi et al. (41) measured a reduced scattering coefficient $\mu_s' \sim 70 \text{ cm}^{-1}$ at 450 nm. Based on their fitting curves, we could expect a coefficient of $\sim 90 \text{ cm}^{-1}$ at 410 nm. The authors conclude that strong and efficient scattering in dermis is due to a high concentration of collagen fibrils. As stated above, the reticular layer part of the dermis is a densely packed meshwork of connective tissue and collagen. Achilles tendon has an even higher content of collagen material that is axially oriented.

Our observations and measurements are in good agreement with the reduced scattering coefficients for similar tissues. The highest level of backscattering was observed for thin samples with intralipid emulsion on top, followed by Achilles tendon, and skeletal muscle showing very weak backscattering.

DISCUSSION

To complement the shortcomings of fluorescence microscopy, other nonlinear optical imaging techniques are available. Of particular interest is second-harmonic generation (SHG) due to its specificity to noncentrosymmetric structures. In our study, we focus on SHG imaging of collagen scaffolds of fascia and Achilles tendon. Histologically, both structures present very similar collagen arrays but different densities (39,45,46).

In second-harmonic generation, as a coherent process, light is generated anisotropically due to wavevector mismatch. Therefore, the forward signal is stronger than the backward signal (20,21). Our results confirm this well-known phenomenon for fascia and Achilles tendon and are summarized in Table 1. In our study, the F/B ratios were measured to determine the fraction of forward signal contributing to the overall backward signal due to backscattering. The five-times higher F/B value obtained for Achilles tendon

TABLE 1 Summary of the measurements from Figs. 2 and 3

Description	F/B	LE/B	T/B	P_{bs} % (lipid emulsion)	P_{bs} % (intact thick ex vivo tissue)
Achilles tendon	24.9 (2.4)	10.6 (1.4)	6.2 (0.8)	39 (10)	21 (6)
Fascia	4.2 (0.1)	2.7 (0.2)	1.1 (0.4)	41 (7)	2 (11)

The measurement errors are in brackets ($\pm$). F, signal in the forward direction. B, signal in the backward direction from a thin sample (thickness $\sim 10 \ \mu m$). LE: signal in the backward direction for a thin sample with 20% intralipid emulsion added on top. T, signal in the backward direction from intact tissue block (thickness of ~ 5 mm). P_{bs}, fraction of forward signal contributing to the overall backward signal due to backscattering. The ratios F/B, LE/B, and T/B are outlined in Experimental Methods.

compared to fascia suggests a difference in the density of bundles or bundle size of the collagen scaffolds. To explain the F/B differences in more details and to interpret these ratios, further investigations are necessary.

For thin sample imaging of fascia and Achilles tendon, in addition to a lower SHG signal in backward, the image features are decidedly different compared to the ones obtained in the backward direction. Collagen tissue matrix is highly heterogeneous at the submicron scale and therefore gives rise to a backward image of heterogeneous submicron features (see Fig. 1 c, Fig. 2 b, and Fig. 3 b). These backward images clearly show the boundaries and dimensions of the collagen sheets.

In vivo as well as whole ex vivo thick tissue imaging requires signal collection in the backward direction. It has been suggested (47,48) and demonstrated that backscattering of forward components is the main contribution to the signal for in vivo CARS and THG microscopy (26,28) due to a very large F/B ratio. Through linear scattering, part of the forward components generated in focus are redirected backward and collected. In contrast, SHG imaging of collagen arrays give rise to much smaller F/B ratios. Therefore, the direct backward signal significantly contributes to the image formation. Due to the vastly different features of forward and backward images, it is essential to understand backscattering of forward components for SHG in vivo and thick tissue imaging. This is evident comparing Fig. 2 d (whole Achilles tendon) and Fig. 3 d (intact muscle tissue block with fascia still attached), with Achilles tendon images containing backscattered forward features and fascia containing only direct backward features. Histologically, both structures appear nearly identical.

In our article, we mimic backscattering by adding 20% intralipid emulsion on top of thin samples of Achilles tendon and fascia. We determine the ratios for Achilles tendon, LE/B = 10.6 and fascia LE/B = 2.7. From these ratios, we determine the fraction of forward signal contributing to the overall backward signal due to backscattering. For fascia, 41% of the forward signal is collected in the backward direction. For Achilles tendon, we determine 39%. Considering the error bars of our measurements, these values are nearly equal (see Table 1) as the emulsion provides equal

scattering. The higher LE/B ratio for Achilles tendon is due to a higher F/B ratio. We conclude that, given the same scattering medium, the deciding factor for image formation is the F/B ratio.

We have to address whether the 20% intralipid emulsion affects the SHG signal strength produced in focus. To rule this out, we investigate the backscattering contribution as the intralipid emulsion is not in direct contact with the thin samples. The sample was kept in PBS, sandwiched between two coverslips and the emulsion added on top of the second coverslip. With that approach, ~33% of the forward signal is collected in the backward direction, a result close to the value obtained with direct sample contact (see Table 1).

The slightly lower value is explained by the additional thickness of the coverslip (~100 μm) moving the scattering media further away from the collecting objective, which, in turn, reduces the collection of scattered light. By adding a second coverslip, a larger field of view is required to collect the same amount of light (26) as the generated light after the focus is diverging. We can conclude that direct contact of the emulsion with the sample does not affect significantly the amount of SHG light produced in focus.

Efficient collection of the backscattered components depends on the microscope setup; mainly the characteristics of the objective (26), and the distance between the detector and the objective (12). On a different setup, different probabilities of backscattering may be measured.

We investigate backscattering for the whole, intact tissues, fascia, muscle, and Achilles tendon by imaging thick ex vivo tissue blocks. As expected, backscattering is important for Achilles tendon as collagen fibrils are known to efficiently scatter light (41,49); the fraction of forward signal contributing to the overall backward signal is 21% for Achilles tendon (see Table 1). For fascia, the fraction is only 2%. The reason why we do not observe any forward features for fascia can only be attributed to the following: 1), the thickness of fascia itself cannot provide enough length to backscatter effectively; and 2), the surrounding tissue environment of fascia, mainly skeletal muscle, provides low backscattering as the reduced scattering coefficient for muscle is small (44). For skeletal muscle, we determine that the fraction of forward signal contributing to the overall backward signal is 0.8%. Since the F/B ratio for fascia is small (4.2) and that backscattering in muscle is weak, the main contribution to the image formation is the direct backward signal. For skeletal muscle, with a high F/B ratio (478), the 0.8% of backscattered forward signal is a main contributor to the overall backward signal. For live in vivo imaging of skeletal muscle, backscattering may be higher due to circulating blood flow and fibrillation causing density fluctuations.

For tissues that exhibit very large F/B ratios, even weak backscattering of the forward components will contribute greatly to the image formation. We observed this for SHG imaging of skeletal muscle, and it was recently reported for THG and CARS microscopy (26,28). For tissues with small F/B ratios, the direct backward signal is the main contributor

to the image formation when backscattering is weak. This is exemplified in our study on fascia. Analyzing quantitatively SHG, THG, and CARS in vivo and whole, thick tissue images requires the understanding of linear optical properties. In focus, the interaction of the laser light with tissue is nonlinear. After that, the propagation of the generated light depends solely on the linear optical properties of the surrounding tissue.

For in vivo as well as thick tissue imaging, the resulting image is either an amalgamation of backscattered forward and backward signal or backward alone. The forward and backward signals provide different, but complementary information about the imaged tissue structure, and can be important to interpret different physiological and pathological processes. As discussed above, the forward signal primarily reveals the fibrillar nature of collagen matrices and allows us to discern the various sizes of collagen bundles as well as their directionality. This opens up the possibility to track and investigate changes in size, diameter, or overall shape of individual bundles within tissue structures. The backward signal contains information about the level of structural submicron heterogeneity. Smallest changes that affect or alter the submicron structure of the collagen type I architecture can be monitored or assayed; i.e., changes in tissue boundaries, densities, or even composition of collagen arrays. In addition to imaging direct changes of collagen structures, changes in the backscattering properties of the imaged and the surrounding tissue environment can be determined.

CONCLUSION

Fascia, skeletal muscle, and corresponding tendon can be elegantly studied using SHG. The resulting SHG images provide detailed structural information about collagen scaffolds and skeletal muscle and elicit important aspects about the surrounding tissue properties. The forward components reveal the fibrillar structure of collagen type I architectures. The backward components provide insight into the submicron architecture and the level of structural heterogeneity. In vivo and whole thick imaging requires backward detection scheme. The images obtained for in vivo or intact thick tissue strongly depend on the linear optical properties of the surrounding tissue environment. Those properties determine the contribution of the backscattered forward signal to the image formation. Our study clearly demonstrates that the variation in the scattering properties of tissues strongly affect SHG image formation.

REFERENCES

1. Denk, W., J. H. Strickler, and W. B. Webb. 1990. Two-photon laser scanning fluorescence microscopy. *Science*. 248:73–76.

2. Svoboda, K., W. Denk, D. Kleinfeld, and D. W. Tank. 1997. In vivo dendritic calcium dynamics in neocortical pyramidal neurons. *Nature*. 385:161–165.

3. Miller, M. J., S. H. Wei, I. Parker, and M. D. Cahalan. 2002. Two-photon imaging of lymphocyte motility and antigen response in intact lymph node. *Science*. 296:1869–1873.

4. Larson, D. R., W. R. Zipfel, R. M. Williams, S. W. Clark, M. P. Bruchez, F. W. Wise, and W. W. Webb. 2003. Water-soluble quantum dots for multiphoton fluorescence imaging in vivo. *Science*. 300: 1434–1436.

5. Stosiek, C., O. Garaschuk, K. Holthoff, and A. Konnerth. 2003. In vivo two-photon calcium imaging of neuronal networks. *Proc. Natl. Acad. Sci. USA*. 100:7319–7324.

6. Voura, E. B., J. K. Jaiswal, H. Matoussi, and S. M. Simon. 2004. Tracking metastatic tumor cell extravasation with quantum dot nanocrystals and fluorescence emission-scanning microscopy. *Nat. Med.* 10: 993–998.

7. Centonze, V. E., and J. G. White. 1998. Multiphoton excitation provides optical sections from deeper within scattering specimens than confocal imaging. *Biophys. J.* 75:2015–2024.

8. Brown, E. B., R. B. Campbell, Y. Tsuzuki, L. Xu, P. Carmeliet, D. Fukumura, and R. K. Jain. 2001. In vivo measurement of gene expression, angiogenesis and physiological function in tumors using multiphoton laser scanning microscopy. *Nat. Med.* 7:864–868.

9. Levene, M. J., D. A. Dombeck, K. A. Kasichke, R. P. Molloy, and W. W. Webb. 2004. In vivo multiphoton microscopy of deep brain tissue. *J. Neurophysiol.* 91:1908–1912.

10. Bacskai, B. J., G. A. Hickey, J. Skoch, S. T. Kajdasz, Y. Wang, G. F. Huang, C. A. Mathis, W. E. Klunk, and B. T. Hyman. 2003. Four-dimensional multiphoton imaging of brain entry, amyloid binding, and clearance of an amyloid-β ligand in transgenic mice. *Proc. Natl. Acad. Sci. USA*. 100:12462–12467.

11. Spires, T. L., M. Meyer-Luehmann, E. A. Stern, P. J. McLean, J. Skoch, P. T. Nguyen, B. J. Bacskai, and B. T. Hyman. 2005. Dendritic spine abnormalities in amyloid precursor protein transgenic mice demonstrated by gene transfer and intravital multiphoton microscopy. *J. Neurosci.* 25:7278–7287.

12. Zipfel, W. R., R. M. Williams, and W. W. Webb. 2003. Nonlinear magic: multiphoton microscopy in the biosciences. *Nat. Biotechnol.* 21:1369–1377.

13. Brown, E., T. McKee, E. diTomaso, A. Pluen, B. Seed, Y. Boucher, and R. K. Jain. 2003. Dynamic imaging of collagen and its modulation in tumors in vivo using second-harmonic generation. *Nat. Med.* 9: 796–800.

14. Maiti, S., J. B. Shear, R. M. Williams, W. R. Zipfel, and W. W. Webb. 1997. Measuring serotonin distribution in live cells with three-photon excitation. *Science*. 275:530–532.

15. Flesken-Nikitin, A., R. M. Williams, W. R. Zipfel, W. W. Webb, and A. Y. Nikitin. 2005. Use of multiphoton imaging for studying cell migration in the mouse. *Methods Mol. Biol.* 294:335–345.

16. Dunn, K. W., and P. A. Young. 2006. Principles of multiphoton microscopy. *Nephron Exp. Nephrol.* 103:33–40.

17. Campagnola, P. J., A. C. Millard, M. Terasaki, P. E. Hoppe, C. J. Malone, and W. A. Mohler. 2002. Three-dimensional high-resolution second-harmonic generation imaging of endogenous structural proteins in biological tissues. *Biophys. J.* 82:493–508.

18. Zoumi, A., A. Yeh, and B. J. Tromberg. 2002. Imaging cells and extracellular matrix in vivo by using second-harmonic generation and two-photon excited fluorescence. *Proc. Natl. Acad. Sci. USA*. 99: 11014–11019.

19. Campagnola, P. J., and L. M. Loew. 2003. Second-harmonic imaging microscopy for visualizing biomolecular arrays in cells, tissues and organisms. *Nat. Biotechnol.* 21:1356–1360.

20. Zipfel, W. R., R. M. Williams, R. Christie, A. Y. Nikitin, B. T. Hyman, and W. W. Webb. 2003. Live tissue intrinsic emission microscopy using multiphoton-excited native fluorescence and second harmonic generation. *Proc. Natl. Acad. Sci. USA*. 100:7075–7080.

21. Williams, R. M., W. R. Zipfel, and W. W. Webb. 2005. Interpreting second-harmonic generation images of collagen I fibrils. *Biophys. J.* 88:1377–1386.

22. Plotnikov, S., V. Juneja, A. B. Isaacson, W. A. Mohler, and P. J. Campagnola. 2006. Optical clearing for improved contrast in second harmonic generation imaging of skeletal muscle. *Biophys. J.* 90:328–339.

23. Plotnikov, S. V., A. C. Millard, P. J. Campagnola, and W. A. Mohler. 2006. Characterization of the myosin-based source for second-harmonic generation from muscle sarcomeres. *Biophys. J.* 90:693–703.

24. Chu, S.-W., S.-Y. Chen, G.-W. Chern, T. H. Tsai, Y. C. Chen, B.-L. Lin, and C.-K. Sun. 2004. Studies of $\chi^{(2)}/\chi^{(3)}$ tensors in submicron-scaled bio-tissues by polarization harmonics optical microscopy. *Biophys. J.* 86:3914–3922.

25. Oron, D., D. Yelin, E. Tal, S. Raz, R. Fachimara, and Y. Silberberg. 2004. Depth-resolved structural imaging by third-harmonic generation microscopy. *J. Struct. Biol.* 147:3–11.

26. Débarre, D., W. Supatto, A. M. Pena, A. Fabre, T. Tordjmann, L. Combettes, M. C. Schanne-Klein, and E. Beaurepaire. 2006. Imaging lipid bodies in cells and tissues using third-harmonic generation microscopy. *Nature Meth.* 3:47–53.

27. Wang, H., Y. Fu, P. Zickmund, R. Shi, and J. X. Cheng. 2005. Coherent anti-stokes Raman scattering imaging of axonal myelin in live spinal tissues. *Biophys. J.* 89:581–591.

28. Evans, C. L., E. O. Potma, M. Puoris'haag, D. Coté, C. P. Lin, and X. S. Xie. 2005. Chemical imaging of tissue in vivo with video-rate coherent anti-Stokes Raman scattering microscopy. *Proc. Natl. Acad. Sci. USA*. 102:16807–16812.

29. Roth, S., and I. Freund. 1979. Second harmonic generation in collagen. *J. Chem. Phys.* 70:1637–1643.

30. Brown, R. M., Jr., A. C. Millard, and P. J. Campagnola. 2003. Macromolecular structure of cellulose studied by second-harmonic generation imaging microscopy. *Opt. Lett.* 28:2207–2209.

31. Millard, A. C., P. J. Campagnola, W. Mohler, A. Lewis, and L. M. Loew. 2003. Second harmonic imaging microscopy. *Methods Enzymol.* 361:47–69.

32. Konig, K., and I. Riemann. 2003. Imaging of cardiovascular structures using near-infrared femtosecond multiphoton laser scanning microscopy. *J. Biomed. Opt.* 8:432–439.

33. Alexakis, C., P. Maxwell, and G. Bou-Gharios. 2006. Organ-specific collagen expression: implications for renal disease. *Nephron Exp. Nephrol.* 102:71–75.

34. Diez, J., A. Gonzales, B. Lopez, and R. Querejeta. 2005. Mechanisms of disease: pathologic structural remodeling is more than adaptive hypertrophy in hypertensive heart disease. *Nature Clin. Pract. Cardiovasc. Med.* 2:209–216.

35. Gordon, M. K., and B. R. Olsen. 1990. The contribution of collagenous proteins to tissue-specific matrix assemblies. *Curr. Opin. Cell Biol.* 2: 833–838.

36. Olsen, B. R. 1995. New insights into the function of collagens from genetic analysis. *Curr. Opin. Cell Biol.* 7:720–727.

37. Cutroneo, K. R. 2003. How is type-I procollagen synthesis regulated at the gene level during tissue fibrosis. *J. Cell. Biochem.* 90:1–5.

38. Rasband, W. S. 1997–2006. ImageJ, U. S. National Institutes of Health, Bethesda, Maryland, http://rsb.info.nih.gov/ij/.

39. Canty, E. G., and K. E. Kadler. 2005. Procollagen trafficking, processing and fibrillogenesis. *J. Cell Sci.* 118:1341–1353.

40. Zhang, G., B. B. Young, Y. Ezura, M. Favata, L. J. Soslowsky, S. Chakravarti, and D. E. Birk. 2005. Development of tendon structure and function: regulation of collagen fibrillogenesis. *J. Musculoskelet. Neuronal Interact.* 5:5–21.

41. Saidi, I. S., S. L. Jacques, and F. K. Tittel. 1995. Mie and Rayleigh modeling of visible-light scattering in neonatal skin. *Appl. Opt.* 34:7410–7418.

42. Chen, C., J. Q. Lu, H. Ding, K. M. Jacobs, Y. Du, and X.-H. Hu. 2006. A primary method for determination of optical parameters of turbid samples and application to intralipid between 550 and 1630 nm. *Opt. Exp.* 14:7420–7435.

43. van Staveren, H. J., C. J. M. Moes, J. van Marle, S. A. Prahl, and M. J. C. van Gemert. 1991. Light scattering in intralipid-10% in the wavelength range of 400–1100 nm. *Appl. Opt.* 30:4507–4514.

44. Marquez, G., L. V. Wang, S.-P. Lin, J. A. Schwartz, and S. L. Thomsen. 1998. Anisotropy in the absorption and scattering spectra of chicken breast tissue. *Appl. Opt.* 37:798–804.

45. Borg, T. K., and J. B. Caulfield. 1980. Morphology of connective tissue in skeletal muscle. *Tissue Cell.* 12:197–207.

46. Hohmann, G., T. Pufe, M. Tsokos, T. Zantop, F. Paulsen, and B. Tillmann. 2004. Structure of the human posterior tibial tendon. *Arch. Orthop. Trauma Surg.* 124:237–242.

47. Jiang, Y., I. V. Tomov, Y. Wang, and Z. Chen. 2005. Second-harmonic optical coherence tomography. *Appl. Phys. Lett.* 86:133901.

48. Han, M., G. Giese, and J. F. Bille. 2005. Second harmonic generation imaging of collagen fibrils in cornea and sclera. *Opt. Exp.* 13:5791–5797.

49. Richards-Kortum, R., and E. Sevick-Muraca. 1996. Quantitative optical spectroscopy for tissue diagnosis. *Annu. Rev. Phys. Chem.* 47:555–606.